Elevated TCA cycle function in the pathology of diet-induced hepatic insulin resistance and fatty liver[S]

Santhosh Satapati,[1,*] Nishanth E. Sunny,[1,*] Blanka Kucejova,[*] Xiaorong Fu,[*] Tian Teng He,[*] Andrés Méndez-Lucas,[†] John M. Shelton,[§] Jose C. Perales,[†] Jeffrey D. Browning,[*] and Shawn C. Burgess[2,*,]**

Advanced Imaging Research Center,[*] Department of Pathology,[§] and Department of Pharmacology,[**] University of Texas Southwestern Medical Center, Dallas, TX; and Biophysics Unit,[†] Departament de Ciències Fisiològiques, Universitat de Barcelona, Barcelona, Spain

Abstract **The manner in which insulin resistance impinges on hepatic mitochondrial function is complex. Although liver insulin resistance is associated with respiratory dysfunction, the effect on fat oxidation remains controversial, and biosynthetic pathways that traverse mitochondria are actually increased. The tricarboxylic acid (TCA) cycle is the site of terminal fat oxidation, chief source of electrons for respiration, and a metabolic progenitor of gluconeogenesis. Therefore, we tested whether insulin resistance promotes hepatic TCA cycle flux in mice progressing to insulin resistance and fatty liver on a high-fat diet (HFD) for 32 weeks using standard biomolecular and in vivo $^{2}H/^{13}C$ tracer methods. Relative mitochondrial content increased, but respiratory efficiency declined by 32 weeks of HFD. Fasting ketogenesis became unresponsive to feeding or insulin clamp, indicating blunted but constitutively active mitochondrial β-oxidation. Impaired insulin signaling was marked by elevated in vivo gluconeogenesis and anaplerotic and oxidative TCA cycle flux. The induction of TCA cycle function corresponded to the development of mitochondrial respiratory dysfunction, hepatic oxidative stress, and inflammation. Thus, the hepatic TCA cycle appears to enable mitochondrial dysfunction during insulin resistance by increasing electron deposition into an inefficient respiratory chain prone to reactive oxygen species production and by providing mitochondria-derived substrate for elevated gluconeogenesis.**—Satapati, S., N. E. Sunny, B. Kucejova, X. Fu, T. T. He, A. Méndez-Lucas, J. M. Shelton, J. C. Perales, J. D. Browning, and S. C. Burgess. **Elevated TCA cycle function in the pathology of diet-induced hepatic insulin resistance and fatty liver.** ***J. Lipid Res.*** **2012.** 53: **1080–1092.**

Supplementary key words tricarboxylic acid cycle • fatty acid/metabolism • inflammation • mitochondria • obesity; gluconeogenesis • oxidative stress • nonalcoholic fatty liver disease

Hepatic insulin resistance occurs in the setting of elevated intracellular lipid content, with pathologic oxidative metabolism playing a likely, but poorly understood, role in this association (1–10). This ambiguity is highlighted by seemingly contradictory views of lipid oxidation during hepatic insulin resistance. One view emerged from the discovery that small molecule byproducts of impaired or incomplete lipid catabolism (diacylglycerol, ceramides, acyl-CoA) antagonize insulin action via protein kinase-C (PKC)-dependent phosphorylation of the insulin receptor substrate (IRS) in skeletal muscle (1–4). Impaired lipid oxidation has also been proposed in the insulin-resistant liver, providing a plausible mechanism for the strong association between hepatic insulin resistance and nonalcoholic fatty liver disease (NALFD) (2, 3, 6, 7). However, a second view, developed mainly in the context of NAFLD, posits that elevated lipid burden stimulates hepatic fat oxidation and results in excessive formation of reactive oxygen species (ROS) (5, 8–10). The resulting oxidative stress and organelle damage may play a critical role in the progression from benign NAFLD to inflammatory nonalcoholic steatohepatitis (NASH) and cirrhosis (10, 11). In the

Support for this work was provided by National Institutes of Health Grant RO1-DK-078184 (to S. C. B.) and American Diabetes Association Grant 7-09-BS-24 (to S. C. B.). Core support was provided by National Institutes of Health Grants UL1-DE-019584, RR-02584, and P01-DK058398. A.M. was supported by a travel grant from the Ministry of Science and Innovation, Spain (BFU2009-07506). Histology was performed by the Molecular Pathology Core at the University of Texas Southwestern Medical Center. The contents of this work are solely the responsibility of the authors and do not necessarily represent the official views of the National Institutes of Health or other granting agencies.

Manuscript received 8 December 2011 and in revised form 29 March 2012.

Published, JLR Papers in Press, April 8, 2012
DOI 10.1194/jlr.M023382

Abbreviations: EGP, endogenous glucose production; Foxo1, forkhead transcription factor 1; GNG, gluconeogenesis; GLY, glycogenolysis; HE, hematoxylin; HFD, high-fat diet, IRS, insulin receptor substrate; MAG, monoacetone glucose; NALFD, nonalcoholic fatty liver disease; NASH, nonalcoholic steatohepatitis; PC, pyruvate carboxylase; PEP, phosphoenolpyruvate; PEPCK, PEP carboxykinase; PKC, protein kinase-C; RCR, respiratory control ratio; ROS, reactive oxygen species; TBARS, thiobarbituric acid reactive substance; TCA, tricarboxylic acid.

[1] S. Satapati and N. E. Sunny contributed equally to this work.

[2] To whom correspondence should be addressed.
e-mail: shawn.burgess@utsouthwestern.edu

[S] The online version of this article (available at http://www.jlr.org) contains supplementary data in the form of one figure and seven tables.

context of hepatic insulin resistance, excessive oxidative metabolism is sufficient to activate inflammatory pathways, which further disrupt insulin action (5, 9, 12–16).

Despite disagreement regarding the link between hepatic insulin resistance, lipid oxidation, and fatty liver, mitochondrial respiratory dysfunction is a common corollary in most models of chronic hepatic insulin resistance. Individuals with NASH have hepatic mitochondria with ultrastructural and respiratory chain damage (8, 17), and high-fat diet (HFD) mice have mitochondria with reduced respiratory efficiency, which promotes ROS-mediated hepatocellular damage (18). In humans, poorly coupled respiration is recapitulated as impaired hepatic ATP turnover during NASH and diabetes (19, 20). The development of respiratory dysfunction and ROS production has been directly linked to impaired hepatic insulin action via forkhead transcription factor 1 (Foxo1) activity, which results not only in upregulation of gluconeogenic and oxidative genes (21) but also in heme-catabolizing enzymes that damage respiratory complexes (22, 23). However, even a clear role for respiratory dysfunction does little to clarify oxidative function in the insulin-resistant liver. Impaired insulin action predicts elevated oxidative metabolism (via PGC-1α, for example) (21), and uncoupled respiration should theoretically increase oxidative metabolism. Several ex vivo studies of mitochondria from HFD mice confirm elevated respiration (24–27), which may increase oxygen consumption and predispose liver to hypoxia (18). However, other studies implicate respiratory dysfunction in the deactivation of surtuins and PGC-1α, which in turn suppress hepatic fat oxidation and cause hepatic steatosis (22, 23, 28, 29). Unfortunately, most conclusions have been based on ex vivo mitochondrial respiration or fat oxidation, leaving the physiologic function of hepatic oxidative metabolism during insulin resistance unclear.

The tricarboxylic acid (TCA) cycle links fat oxidation to respiration by converting acetyl-CoA to CO_2 and harvesting electrons as 3NADH and a $FADH_2$ for respiratory complexes 1 and 2, respectively. The activity of TCA cycle oxidation is acutely regulated by cellular energy charge and redox state, which precisely matches NADH production to respiratory demand (30, 31). A unique feature of liver mitochondria is that the hepatic TCA cycle is not requisitely yoked to β-oxidation because acetyl-CoA in excess of cellular energy demand is shunted to ketogenesis. Thus, the TCA cycle remains matched to cellular respiratory demand, whereas ketogenesis dissipates excess acetyl-CoA into ketones for peripheral oxidation, while also reducing the gluconeogenic burden of the liver (30, 31). Another specialized feature of the hepatocellular TCA cycle is that it harbors prominent anaplerotic and cataplerotic (nonoxidative) pathways required for gluconeogenesis, lipogenesis, and ureagenesis (32). These pathways are upregulated by insulin resistance (33–35), but their functions are rarely recapitulated during ex vivo examination of mitochondrial oxidative/respiratory metabolism. Pyruvate carboxylase (PC) and phosphoenolpyruvate (PEP) carboxykinase (PEPCK) are the archetypal anaplerotic and cataplerotic enzymes of liver that are required for gluconeogenesis, and modified versions of these pathways are also required for lipogenesis and amino acid metabolism (32). Anaplerosis/cataplerosis is a substantial pathway in liver, roughly 3- to 5-fold more active than oxidative TCA cycle flux (36). Thus, the hepatic TCA cycle is semiautonomous of β-oxidation and intimately linked to biosynthesis and cellular respiration, but its function during insulin resistance is unknown.

Given the putative link between insulin resistance, elevated gluconeogenesis, and loss of mitochondrial respiratory integrity, we hypothesized that impaired insulin signaling should result in increased oxidative and anaplerotic/cataplerotic fluxes of the TCA cycle. Hepatic metabolism was examined in mice after 8, 16, and 32 weeks of a HFD using standard biomolecular methods and $^{2}H/^{13}C$ tracers of hepatic metabolism. Hepatic mitochondrial content, respiration, metabolomic markers of β-oxidation, and in vivo metabolic flux in TCA cycle pathways were elevated with loss of hepatic insulin action. Mitochondrial uncoupling, oxidative stress, and inflammation developed synchronously with the induction of oxidative TCA cycle flux. The findings indicate that loss of hepatic insulin action induces TCA cycle flux, which in the setting of impaired respiratory efficiency may contribute to oxidative stress and ultimately inflammation.

MATERIALS AND METHODS

Animals and diets

Animal protocols were approved by the Institutional Animal Care and Use Committee at the University of Texas Southwestern Medical Center. Four- to six-week-old male C57Bl/6 mice (Charles River) were fed either a control semisynthetic diet (10% fat calories; Teklad diet TD06416; Harlan Laboratories) or a high-fat diet (60% fat calories; Teklad diet TD06414; Harlan Laboratories) for 8, 16, or 32 weeks to induce obesity and insulin resistance. Experiments were carried out after an overnight fast (~16 h) unless otherwise noted.

Stable isotope tracer infusions

Mice were surgically implanted with indwelling jugular vein catheters and allowed to recover for five days. Following an overnight fast, unrestrained mice were infused with [3,4-$^{13}C_2$]acetoacetate and [U-$^{13}C_4$]sodium β-hydroxybutyrate as a bolus (8.8 and 6.7 μmol/hr) for 10 min and as a continuous infusion (3.5 and 2.7 μmol/hr) for a further 80 min (26). At the end of 90 min, approximately 50 μl of blood was collected for LC-MS/MS analysis of ketone turnover (26). Mice then received an intraperitoneal injection of isotonic D_2O (99%; 28 μl/ body weight) and administration of [U-$^{13}C_3$]propionate (50 mg/ml) and [3,4-$^{13}C_2$] glucose (3.72 mg/ml) as a bolus (6.1 μmol/hr) for the first 10 min and continuous (1.2 μmol/hr) for the next 80 min. After mice were anesthetized, whole blood was collected from the descending aorta, and tissues were collected and stored at −80°C until further analysis.

LC-MS/MS analysis of ketone tracer dilution

Thawed blood was immediately spiked with an equal volume of 1M NaB^2H_4 to convert labile acetoacetate (ACAC) to stabile β-hydroxybutyrate (BHB), with the deuterium tag (M+1), preserving its source as acetoacetate (37). Samples were purified by ion

exchange chromatography and analyzed on a API 3200 triple quadrupole LC-MS/MS (Applied Biosystems/Sciex Instruments) under positive ionization to determine enrichments of β-hydoxybutyrate mass isotopomers (26). The following MRM transitions were monitored to quantify β-hydroxybutyrate isotopomers. These data were fit to a two-pool model of ketone turnover (38).

Detection of β-hydroxybutyrate originating from:
β-hydroxybutyrate 105/87 (M+0)
Reduced acetoacetate 106/88 (M+1)
[3,4-^{13}C]β-hydroxybutyrate 107/89 (M+2)
Reduced [3,4-^{13}C]acetoacetate 108/90 (M+3)
[1,2,3,4-^{13}C]β-hydroxybutyrate 109/91 (M+4)
Reduced [1,2,3,4-^{13}C]acetoacetate 110/92 (M+5)

Assumptions, limitations and validation of apparent ketone turnover as an indicator of ketogenesis have been evaluated by us (26, 39) and others (37, 38). Briefly, this methodology hinges on the assumption that ketone tracers are only diluted by ketone production by liver or exchange between β-hydroxybutyrate and acetoacetate. There appears to be an unknown degree of dilution by extrahepatic tissues, termed pseudoketogenesis, which cannot be quantified by tracer methodology (37), but it appears to be small as A/V differences agree with tracer dilution (38). In rodents, we found ketone turnover to be very sensitive to nutritional, pharmacologic, and genetic manipulation of hepatic fat oxidation (26, 39).

Isotopomer analysis by NMR

Whole blood (~0.75 ml) was deproteinized with equal volumes of 0.3N zinc sulfate and 0.3N barium hydroxide and lyophilized. Blood glucose was converted to 1,2-isopropylidene glucofuranose (monoacetone glucose, MAG) (40, 41). MAG was analyzed by ^{2}H and ^{13}C NMR on a 14T NMR INOVA spectrometer with a 3 mm broadband probe (Varian, Palo Alto, CA), and peak areas were integrated using the 1D NMR software ACD/Labs 11.0 (Advanced Chemistry Development, Toronto, Ontario, Canada) as previously described (40, 41).

Endogenous glucose production

Steady state infusion of [3,4-$^{13}C_2$]glucose was used to determine endogenous glucose production (EGP) using the tracer dilution approach (40–42). Briefly, [3,4-$^{13}C_2$]glucose was detected as the C3 D34 signal and the C4 D43 signal. These signals were averaged and compared with a standard curve to determine absolute plasma [3,4-$^{13}C_2$]glucose enrichment.

$$\begin{aligned}\text{EGP (v1)} = {} & (\text{infusate enrichment} \\ & - \text{plasma glucose enrichment}) \\ & /(\text{plasma glucose enrichment}) \\ & /\text{tracer infusion rate}\end{aligned} \quad \textit{(Eq. 1)}$$

Relative gluconeogenesis

The fractional contribution of glycogenolysis (GLY), total gluconeogenesis (GNG), and TCA cycle gluconeogenesis (i.e., via phosphoenolpyruvate) to endogenous glucose production were determined from the relative deuterium enrichments in the H2, H5, and H6s position of MAG (43) as determined by ^{2}H NMR analysis (44). Briefly, H2 enrichment occurs during any source of glucose production (glycogenolysis, gluconeogenesis from glycerol, gluconeogenesis from TCA cycle substrates); H5 enrichment occurs during the triose isomerase reaction during any source of gluconeogenesis; H6s enrichment occurs during gluconeogenesis from TCA cycle substrates (43). Thus fluxes relative to EGP (in hexose units) are:

$$\text{GLY}(\text{v2}/\text{v1}) = 1-(\text{H5} / \text{H2}) \quad \textit{(Eq. 2)}$$

$$\text{GNG from glycerol } (\text{v3}/\text{v1}) = (\text{H5}-\text{H6s}) / \text{H2} \quad \textit{(Eq. 3)}$$

$$\text{GNG from PEP } (\text{v4}/\text{v1}) = (\text{H6s} / \text{H2}) \quad \textit{(Eq. 4)}$$

Relative rates of the TCA cycle

First-pass metabolism of propionate occurs almost exclusively in liver of rodents (45), where it is carboxylated and converted to the TCA cycle intermediate succinyl-CoA. Carbon isotope tracers of propionate have been used to assess relative rates of the hepatic TCA cycle in humans (46, 47) and rodents (39–41). Carbon-13 isotopomers of glucose formed by tracer level TCA cycle metabolism of [U-^{13}C]propionate were quantified by ^{13}C NMR analysis of the C2 resonance of MAG (48), which provided the relative abundance of three isotopomers of glucose: [1,2-^{13}C]glucose, [2,3-^{13}C]glucose, and [1,2,3-^{13}C]glucose, corresponding to the D12, D23, and Q signals of a nine-line multiplet. Isotopomer data were evaluated using a model similar to Magnusson and Landau (36), but it was generated by an independent set of differential equations (49) to determine fluxes of the TCA cycle. Inasmuch as acetyl-CoA and bicarbonate used in the TCA cycle are not labeled, these differential equations reduce to three simple equations (41, 48) for flux through pathways relative to oxidative TCA cycle flux (v7) (in triose units).

$$\text{Pyruvate cycling}/\text{TCA cycle } (\text{v5}/\text{v7}) = (\text{D12}-\text{Q}) / \text{D23} \quad \textit{(Eq. 5)}$$

$$\text{Anaplerosis}/\text{TCA cycle } (\text{v6}/\text{v7}) = (\text{D12}-\text{D23}) / \text{D23} \quad \textit{(Eq. 6)}$$

$$\text{GNG}/\text{TCA cycle } (\text{v4}/\text{v7}) = (\text{Q}-\text{D23}) / \text{D23} \quad \textit{(Eq. 7)}$$

Absolute rates of metabolic flux

See supplemental material for more details. Briefly, equations 1–7 were solved for seven fluxes (v1–v7) as we previously described (41) and as presented in supplementary Table VII. Normalization of the equations assumes that ^{2}H and ^{13}C isotopomers of glucose have common origins in the liver (41).

Palmitate oxidation in liver homogenates

Oxidation of palmitate in the liver of 24 h fasted animals was performed as described by Dohm et al. (50) with few modifications. Briefly, ~500 mg of liver in 2.5 ml of reaction buffer (2 mM ATP, 0.05 mM CoA, 1 mM dithiotreitol, 0.1 mM NAD^{+}, 1 mM DL-carnitine, 0.1 mM malate, 1 mM $MgCl_2$, 0.072 mM fatty acid free BSA, 100 mM sucrose, 10 mM K_2HPO_4, 80 mM KCl, 0.1 mM EDTA, 100 mM HEPES pH 7.3) was homogenized in a hand-operated Potter-Elvehjem homogenizer by 15 strokes. Reaction was started by adding 3 μl of [1-^{14}C] palmitate (0.3 mCi, final 25 mM; PerkinElmer) to 200 μl of homogenate and incubated at 37°C for 4, 5, 6, and 7 min. Palmitate oxidation was terminated by injecting 100 μl of 7% $HClO_4$ followed by centrifugation at 15,000 *g* for 10 min. Then 200 μl of supernatant was counted for incorporation of ^{14}C into acid soluble molecules in 6 ml of scintillation liquid. After conversion to DPM, oxidation rate was calculated as nanomoles of palmitate per minute per milligram of tissue and then per whole liver.

Hepatic insulin resistance

Progression of hepatic insulin resistance on a high-fat diet was evaluated using the Matsuda index (51). Further qualification of insulin's ability to suppress hepatic ketogenesis was assessed by hyperinsulinemic-euglycemic clamp as we previously described (52) but modified to include [3,4-$^{13}C_2$]acetoacetate and [U-$^{13}C_4$]β-hydroxybutyrate. Briefly, mice were acclimated to a tube holder by daily exposure for 6–8 days prior to the clamp. An initial 90 min of ketone tracer infusion, as described above,

was performed to determine basal fasting ketone turnover. Mice were restrained in a tube holder and insulin (10 mU/kg/min) and ketone tracers were infused at a constant rate. Blood glucose levels were monitored from the tail vein every 10 minutes, and euglycemia was maintained by variable infusion of 30% glucose. After 80 min of hyperinsulinemic euglycemia, steady-state blood ketone enrichments were determined by LC-MS/MS as described above.

LC-MS/MS analysis of liver acylcarnitines and ceramides

Acylcarnitines and ceramides were measured on an API 3200 triple quadrapole LC-MS/MS as previously described (53, 54). Briefly, free carnitine and acylcarnitines were extracted from the liver and derivatized, and then individual acylcarnitine peaks were quantified by comparison with a ^{13}C internal standard (Cambridge Isotopes, Andover, MA) (53). Liver ceramides were extracted by chloroform/methanol extraction and ceramide peaks were quantified by comparison with a ^{13}C internal standard (Cambridge Isotopes) (54). Metabolites were normalized to the liver protein (Thermo Scientific, Rockford, IL).

Hepatic mitochondrial respiration

Crude mitochondria were isolated from the livers of overnight-fasted mice as described previously (55). Mitochondrial loading was estimated from protein content determined from a Bradford assay. Respiration rates were determined at 37°C in 1 ml of reaction buffer (100 mM KCl, 20 mM sucrose, 10 mM KH2PO4, 5 mM HEPES, 2 mM MgCl2-6H2O, 1 mM EGTA, pH 7.2, and 0.5% BSA) using a Clark-type O_2 electrode (Oxygraph Oxygen electrode; Hansatech Instruments, Norfolk, England) with either succinate (2.5 mM), glutamate/malate (5 mM/2.5 mM), or palmitoyl-L-carnitine/malate (20 μM/2.5 mM) as substrates. When using succinate, complex I was inhibited with rotenone (2 μM). State 2 (basal, leak) respiration was measured after addition of 0.66 mg of mitochondria and respiratory substrate, state 3 respiration was induced by adding ADP (150 μM), and state 4 respiration was measured after ADP depletion. Respiratory control ratio (RCR) was calculated as the ratio of state 3 to state 4 respirations. P/O ratio was calculated as the ratio of ATP formed to oxygen consumed. Respiration rates were normalized to citrate synthase activity (Citrate Synthase Assay kit; Sigma-Aldrich, St. Louis, MO).

Gene expression analysis

Total RNA was extracted from tissues with RNA Stat-60 reagent (Tel-Test, Friendswood, TX). cDNA was synthesized from 4 μg of RNA treated with 0.2 U DNase (Qaigen, Valencia, CA) using High Capacity cDNA Reverse Transcription Kit (Applied Biosystems, Carlsbad, CA). Quantitative real-time PCR was run in triplicates using SYBR GreenER™ qPCR SuperMix for ABI PRISM® instrument (Invitrogen, Carlsbad, CA) and ABI PRISM 7900HT Fast Real-Time PCR System (Applied Biosystems). Gene expression was normalized to cyclophilin b (Ppib). Primer sequences will be provided upon request.

Western blot analysis

Frozen livers or crude mitochondria were homogenized in RIPA buffer (Cell Signaling Technology, Danvers, MA) with complete protease inhibitors (Roche Diagnostics, Indianapolis, IN). Proteins were separated with SDS-PAGE and transferred onto a Protran™ nitrocellulose membrane (Whatman/GE Healthcare, Piscataway, NJ) or Immobilon-P PVDF membrane (Millipore, Billerica, MA). Primary antibodies were obtained from Cell Signaling. Mitochondrial carbonylated proteins were assessed using OxiSelect™ Protein Carbonyl Immunoblot Kit (Cell Biolabs, San Diego, CA).

Hepatic mitochondrial DNA content

Total DNA was isolated from the liver using phenol/chloroform/isoamylalcohol (25:4:1) extraction and ethanol precipitation. Quantitative real-time PCR was performed in triplicate using SYBR GreenER™ qPCR SuperMix for ABI PRISM® Instrument (Invitrogen), primers for mitochondrial *mt-Nd2* and nuclear *Ndufv1,* and ABI PRISM 7900HT Fast Real-Time PCR System (Applied Biosystems). Relative DNA content was quantified from Ct values using decimal dilutions of one of the samples as standard curve. Mitochondrial DNA (mtDNA) content is expressed per diploid nucleus.

Histology

Liver from overnight-fasted mice were fixed in methanol-free 4% paraformaldehyde for 20–24 h, cryoprotected with sequential 10% and 18% sucrose equilibrations for 12 h at 4°C, and then cryoembedded in optimal cutting temperature medium (OCT; Sakura Finetek, Torrence, CA). Multiple plane 8 μm thick cryostat sections were prepared and temporarily stored at −80°C. Staining for lipids was conducted using saturated 0.18% Oil Red O (Sigma-Aldrich, St. Louis, MO) prepared in 60% isopropyl alcohol according to established histology protocol. The slides were counterstained with Hematoxylin and cover slips applied using aqueous mounting medium (Vector Laboratories, Inc., Burlingame, CA).

Inflammatory markers

Plasma inflammatory cytokine analysis was performed by the University of Texas Southwestern Metabolic Core using Luminex 100 bead mapping technology (Luminex, Austin, TX).

Biochemical measurements

Blood glucose concentration was measured with a glucometer (Accuchek; Roche Diagnostics, IN). Analytical kits were used to determine liver triglycerides (Sigma-Aldrich, St. Louis, MO), plasma free fatty acids (Wako Chemicals Inc., Richmond, VA), total ketones (Wako Chemicals Inc.), lipid peroxidation in frozen liver homogenates (Cayman Chemical Co., MI) and antioxidant activity of superoxide dismutase (Cayman Chemical Co.). Enzyme-linked immunoassays were used to measure plasma insulin (ALPCO Diagnostics, NH), adiponectin (Millipore Corporation, MA), and leptin (Crystal Chem Inc., IL).

Materials

[3, 4-^{13}C]glucose (98%) was purchased from Omicron Biochemicals (South Bend, IN). [3, 4-$^{13}C_2$]ethylacetoacetate (98%) and [U-$^{13}C_4$]β-hydroxybutyrate (98%) were purchased from Isotec (St. Louis, MO). [U-^{13}C]propionate and deuterium oxide (99%) were purchased from Cambridge Isotopes (Andover, MA). Other common chemicals were obtained from Sigma (St. Louis, MO).

Statistical analysis

All data are presented as the mean ± SE. Differences between groups were analyzed using ANOVA, and pairwise mean comparisons were done using an unpaired *t*-test. Differences were considered significant at $P \leq 0.05$.

RESULTS

HFD results in obesity insulin resistance, hyperglycemia, and fatty liver

The metabolic characteristics of fasted mice maintained on a HFD for up to 32 weeks are presented in **Table 1**. HFD mice had increased body weights at 8 (+30%), 16 (+34%),

TABLE 1. Metabolic characteristics of overnight-fasted mice on a high-fat diet

	8 Weeks		16 Weeks		32 Weeks	
	Control Diet	HFD	Control Diet	HFD	Control Diet	HFD
Body weight (g)	29.3 ± 0.7	38.2 ± 1.5[a]	31.5 ± 1.4	42.4 ± 1.3[a]	38.5 ± 0.7	53.6 ± 1.8[a]
Lean body weight (%)	61.6 ± 0.7	50.0 ± 0.9[a]	56.7 ± 1.4	49.2 ± 1.4[a]	53.2 ± 0.4	45.5 ± 1.9[a]
Body fat (%)	26.0 ± 1.1	42.9 ± 0.70[a]	33.6 ± 1.6	44.3 ± 1.5[a]	37.1 ± 0.3	48.6 ± 2.1[a]
Liver TG (mg/g liver)	81 ± 10	110 ± 12[a]	94.1 ± 25	159 ± 22[a]	132 ± 7	189 ± 25[a]
Glucose (mg/dl)	67.7 ± 2.2	102 ± 6.9[a]	72.5 ± 2.7	116 ± 11[a]	87.7 ± 2.0	135 ± 11[a]
Insulin (ng/ml)	0.41 ± 0.03	1.92 ± 0.32[a]	0.18 ± 0.02	2.2 ± 0.2[a]	0.43 ± 0.05	5.2 ± 0.8[a]
NEFA (μEQ/l)	586 ± 36	697 ± 67	876 ± 82	1129 ± 100[a]	610 ± 71	535 ± 78
Ketone (μmol/l)	1220 ± 104	1179 ± 119	719 ± 126	1189 ± 161[a]	1263 ± 174	789 ± 141[a]
Leptin (ng/ml)	13.2 ± 1.3	83.3 ± 11[a]	45.1 ± 3.5	105 ± 11[a]	33.9 ± 5.5	119 ± 12[a]
Adiponectin (ng/ml)	4297 ± 164	3667 ± 132[a]	3866 ± 72.0	3914 ± 113	3858 ± 86.0	4034 ± 150

Data are represented as the mean ± SE (n = 6–8).
[a]$P \leq 0.05$ between control and high-fat groups.

and 32 (+38%) weeks. Body composition analysis by magnetic resonance indicated that excess body weight was composed mainly of increased adiposity (Table 1). The development of obesity was accompanied by progressing hyperinsulinemia, hyperleptinemia, and hyperglycemia (Table 1). The duration of HFD was associated with increased hepatic steatosis indicated by elevated liver triglyceride content (Table 1) and positive Oil Red O staining (**Fig. 1A**). Increasing hepatic lipid content and the duration of HFD was also associated with a decline in hepatic

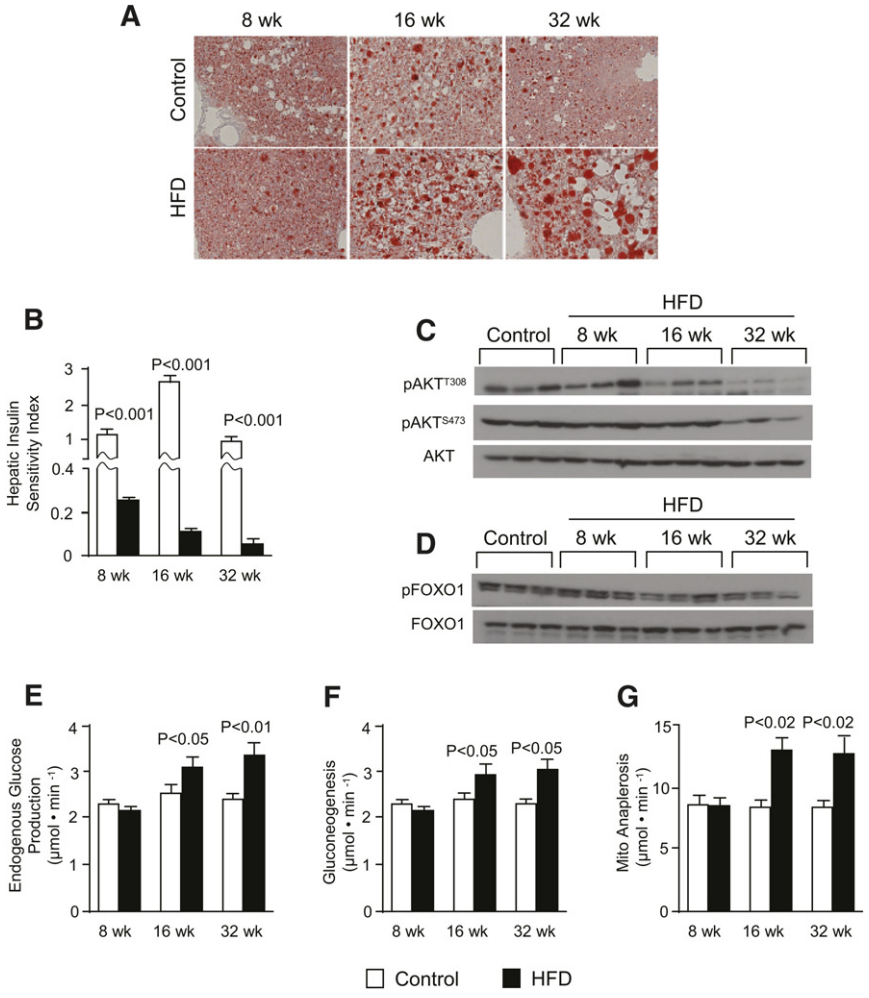

Fig. 1. HFD mice have fatty liver with impaired insulin action. (A) Oil red O-stained liver sections (original magnification ×10; n = 2); (B) hepatic insulin sensitivity index; (C) insulin-stimulated phosphorylation of Akt^{T308} and Akt^{S473}; (D) insulin-stimulated Foxo1 phosphorylation; (E) endogenous glucose production; (F) total gluconeogenesis; and (G) hepatic anaplerosis or pyruvate carboxylase flux in overnight-fasted mice fed either a control or a high-fat diet for 8, 16, and 32 weeks. Data are presented as the mean ± SE (n = 6–8).

insulin sensitivity (Fig. 1B) and blunted hepatic Akt phosphorylation during an insulin challenge (Fig. 1C and supplementary Fig. I-C). However, we noted that Akt phosphorylation was either not different or slightly increased in the absence of an insulin challenge (supplementary Fig. I-A, B). These data confirm that mice fed a HFD in this study exhibited progressing hepatic steatosis and insulin resistance; therefore, they were used to assess the mitochondrial TCA cycle during this process.

Mitochondrial TCA cycle anaplerosis and gluconeogenesis are increased in the liver of HFD mice

Anaplerosis, which refers to the conversion of cytosolic metabolites into mitochondrial TCA cycle intermediates, is a critical pathway for gluconeogenesis and other biosynthetic processes (32). In liver, anaplerosis is governed by mitochondrial PC, an enzyme that converts pyruvate to oxaloacetate and controls the rate of cataplerotic PEPCK flux for gluconeogenesis (56). Because insulin action regulates this process, we evaluated gluconeogenesis and the upstream pathways of mitochondrial anaplerosis and cataplerosis during HFD. Foxo1 phosphorylation was normal after 8 wks but decreased with longer durations of HFD (Fig. 1D). Gene expression analysis (**Table 2**) indicated increased expression of G6Pase after 16 weeks; however, PC and PEPCK were not different or slightly decreased. We further confirmed these findings by Western blotting, which revealed a slight decrease in PEPCK protein (not shown). These data are consistent with other findings in HFD rodents and humans with type 2 diabetes, which did not have elevated hepatic PEPCK (57). Thus, we carefully examined gluconeogenic function by measuring glucose turnover (supplementary Table I and Fig. 1E) with simultaneous administration of ^2H_2O. Relative deuterium enrichments of glucose H2, H5, and H6s were determined by ^2H NMR (supplementary Table II), and these data were used to evaluate the fractional contributions of glycogenolysis, gluconeogenesis from glycerol, and gluconeogenesis from TCA cycle cataplerosis to glucose production (supplementary Table III). Fractional contributions were unremarkable, with the exception of 32-week HFD mice, which had an elevated contribution from glycogenolysis. However, consistent with reduced Foxo1 phosphorylation, fasting endogenous glucose production and total

TABLE 2. Expressions of genes related to carbohydrate, lipid, and mitochondrial metabolism in liver of overnight-fasted mice on a high-fat diet

	8 Weeks		16 Weeks		32 Weeks	
	Control Diet	HFD	Control Diet	HFD	Control Diet	HFD
Glucose production						
Pck1	1.0 ± 0.16	0.6 ± 0.13	1.0 ± 0.10	0.9 ± 0.12	1.0 ± 0.10	0.6 ± 0.07[a]
Pc	1.0 ± 0.17	0.8 ± 0.12	1.0 ± 0.09	1.0 ± 0.10	1.0 ± 0.09	0.6 ± 0.07[a]
G6pase	1.0 ± 0.32	0.9 ± 0.16	1.0 ± 0.19	3.2 ± 0.50[a]	1.0 ± 0.26	1.8 ± 0.52[a]
Mdh1	1.0 ± 0.18	0.6 ± 0.09[a]	1.0 ± 0.08	0.7 ± 0.15[a]	1.0 ± 0.07	0.6 ± 0.07[a]
Foxo1	1.0 ± 0.15	1.0 ± 0.20	1.0 ± 0.09	1.1 ± 0.20	1.0 ± 0.14	1.0 ± 0.09
Glucose transport						
Glut2/ Slc2a2	1.0 ± 0.17	1.1 ± 0.18	1.0 ± 0.11	1.1 ± 0.15	1.0 ± 0.09	0.6 ± 0.07[a]
Fat oxidation and ketogenesis						
Pgc1a/Ppargc1a	1.0 ± 0.17	1.1 ± 0.20	1.0 ± 0.28	1.5 ± 0.27[a]	1.0 ± 0.13	1.1 ± 0.16
Ppara	1.0 ± 0.09	1.2 ± 0.19	1.0 ± 0.15	1.2 ± 0.24	1.0 ± 0.18	0.5 ± 0.08[a]
Cpt1a	1.0 ± 0.18	1.2 ± 0.16	1.0 ± 0.18	1.2 ± 0.21	1.0 ± 0.13	0.5 ± 0.07[a]
Vlcad/Acadvl	1.0 ± 0.13	1.2 ± 0.15	1.0 ± 0.10	0.9 ± 0.17	1.0 ± 0.11	0.9 ± 0.26
Lcad/Acadl	1.0 ± 0.14	1.0 ± 0.13	1.0 ± 0.14	1.0 ± 0.19	1.0 ± 0.15	0.8 ± 0.28
Mcad/Acadm	1.0 ± 0.13	1.3 ± 0.17	1.0 ± 0.11	1.0 ± 0.17	1.0 ± 0.13	1.1 ± 0.16
Cd36/Fat	1.0 ± 0.05	1.0 ± 0.08	1.0 ± 0.13	1.9 ± 0.26	1.0 ± 0.10	0.9 ± 0.10
Hmgcs2	1.0 ± 0.14	0.8 ± 0.07	1.0 ± 0.04	0.8 ± 0.16	1.0 ± 0.07	0.5 ± 0.09[a]
Acc2/Acacb	1.0 ± 0.13	0.8 ± 0.12	1.0 ± 0.21	1.1 ± 0.20	1.0 ± 0.20	2.6 ± 0.33[a]
Kreb's cycle						
Cs	1.0 ± 0.18	0.7 ± 0.14	1.0 ± 0.14	1.1 ± 0.15	1.0 ± 0.13	0.9 ± 0.12
Mitochondrial respiration						
Cycs	1.0 ± 0.34	0.7 ± 0.07	1.0 ± 0.06	1.04 ± 0.079	1.0 ± 0.14	1.1 ± 0.20
Cox4i1	1.0 ± 0.25	0.9 ± 0.15	1.0 ± 0.13	0.8 ± 0.09	1.0 ± 0.14	1.3 ± 0.18
Ucp2	1.0 ± 0.29	1.1 ± 0.15	1.0 ± 0.19	2.6 ± 0.61[a]	1.0 ± 0.08	2.1 ± 0.65[b]
Lipogenesis						
Lxrα/Nr1 h3	1.0 ± 0.06	0.9 ± 0.12	1.0 ± 0.12	0.8 ± 0.12	1.0 ± 0.10	1.6 ± 0.12[a]
Srebp1c/Srebf1	1.0 ± 0.15	1.4 ± 0.19	1.0 ± 0.08	1.9 ± 0.65[a]	1.0 ± 0.11	2.0 ± 0.23[a]
Fasn	1.0 ± 0.11	0.8 ± 0.08	1.0 ± 0.10	1.1 ± 0.15	1.0 ± 0.18	1.0 ± 0.10
Chrebp/Mlxipl	1.0 ± 0.05	0.7 ± 0.10[a]	1.0 ± 0.11	0.7 ± 0.11[a]	1.0 ± 0.14	0.4 ± 0.04[a]
Hmgcr	1.0 ± 0.20	1.0 ± 0.17	1.0 ± 0.11	1.1 ± 0.16	1.0 ± 0.12	0.8 ± 0.12
Hmgcs1	1.0 ± 0.08	1.9 ± 0.15[a]	1.0 ± 0.11	2.2 ± 0.37[a]	1.0 ± 0.10	1.0 ± 0.19
Acc1/Acaca	1.0 ± 0.18	0.9 ± 0.16	1.0 ± 0.09	0.9 ± 0.09	1.0 ± 0.09	0.9 ± 0.10
Glycolysis						
Gck	1.0 ± 0.23	0.6 ± 0.11	1.0 ± 0.09	1.6 ± 0.18[a]	1.0 ± 0.09	1.4 ± 0.21[a]
Pentose phosphate pathway						
G6pdx	1.0 ± 0.17	1.0 ± 0.17	1.0 ± 0.10	1.1 ± 0.17	1.0 ± 0.12	1.0 ± 0.13

Data are represented as the mean ± SE (n = 5).
[a] $P \leq 0.05$ between control and high-fat groups.
[b] $P \leq 0.1$ between control and high-fat groups.

gluconeogenesis were elevated after 16 and 32 weeks of HFD (Fig. 1E, F). Elevated gluconeogenesis was due solely to increased flux from TCA cycle intermediates, with no change in gluconeogenesis from glycerol (supplementary Table VI). Furthermore, carbon-13 NMR isotopomer analysis (supplementary Tables IV–VI) of plasma glucose revealed that absolute anaplerotic/cataplerotic flux of the TCA cycle was elevated by roughly 50% after 16 ($P < 0.02$) and 32 ($P < 0.02$) weeks of HFD (Fig. 1G and supplementary Table VI). Although *Pc* expression was not affected by HFD (Table 2), this enzyme is mainly regulated through allosteric interaction with acetyl-CoA (58), consistent with elevated TCA cycle activity and increased hepatic acetylcarnitine (**Table 3**). Thus, increased TCA cycle anaplerosis contributed to elevated gluconeogenesis during impaired insulin action, perhaps by metabolic or substrate level activation of PC.

In vivo hepatic TCA cycle activity is induced by chronic HFD

Because oxidative and respiratory dysfunction has been implicated in hepatic insulin resistance, we examined hepatic lipid oxidation and oxidative TCA cycle flux in HFD mice. Mice on HFD had high levels of short-chain acylcarnitines (Table 3), which was most striking after 32 weeks for C2 (4-fold), C3 (6-fold), and C4 (3-fold). This finding is consistent with elevated β-oxidation previously described in insulin-resistant muscle (59). The TCA cycle oxidizes acetyl-CoA produced by β-oxidation and provides reducing equivalents (NADH and $FADH_2$) required for respiration and redox coupled reactions. Carbon-13 NMR isotopomer analysis of plasma glucose indicated that the rate of gluconeogenesis relative to the rate of TCA cycle turnover was reduced after 16 weeks of HFD (**Fig. 2A** and supplementary Table V). This finding, combined with a higher absolute rate of gluconeogenesis (Fig. 1E, F) indicated elevated hepatic TCA cycle flux. Integrated analysis of ^{13}C and ^{2}H plasma glucose isotopomers (supplementary Tables I–VI) confirmed a 90% ($P = 0.001$) higher oxidative flux through the hepatic TCA cycle at 16 weeks, which persisted at 32 weeks ($P = 0.03$) of HFD (Fig. 2B). To further confirm elevated fat oxidation, we examined the rate of [1-^{14}C]palmitate oxidation in liver homogenates after 16 weeks of HFD. This experiment corroborated in vivo isotopomer analysis, indicated by a 2-fold increase in ^{14}C incorporation into acid soluble intermediates ($P < 0.05$) and a trend for increased $^{14}CO_2$ ($P = 0.1$) production (Fig. 2C). Taken together, metabolomic analysis, in vivo isotopomer analysis, and ex vivo radio-tracer analysis demonstrated that hepatic oxidative metabolism was elevated in the insulin-resistant and fatty liver after 16–32 weeks of HFD.

Mitochondrial ketogenesis is constitutively active, but blunted, by severe insulin resistance

During fasting, β-oxidation exceeds hepatic respiratory requirements, and the resulting acetyl-CoA in excess of TCA cycle oxidative demand is dissipated into ketogenesis (31). Thus, we examined ketogenesis throughout 32 weeks of a HFD to evaluate overall hepatic β-oxidation in the setting of elevated TCA cycle flux during insulin resistance. Fasting plasma ketone concentration became elevated after 16 weeks (+65%, $P = 0.01$), but it fell below normal after 32 weeks of HFD (−38%, $P = 0.03$) (Table 1). Likewise, apparent ketone turnover was higher after 16 weeks ($P = 0.05$) but slightly lower after 32 weeks of HFD ($P = 0.02$) (Fig. 2D). These data were consistent with ex vivo rates of palmitate oxidation (Fig. 2C) and the induction of hepatic *Pgc1α* after 16 weeks, followed by the downregulation of *Pparα*, *Cpt1a*, and *Hmgcs2* after 32 weeks (Table 2). Thus, in agreement with our previous findings (26, 39), fasting ketone turnover is increased with moderate insulin resistance but is impaired by severe insulin resistance.

Blunted fasting ketogenesis after 32 weeks of HFD contrasted with elevated oxidative TCA cycle flux, so we further tested whether this pathway was appropriately regulated by nutritional state and insulin action. Control mice suppressed fasting ketogenesis by 40-fold during a hyperinsulinemic-euglycemic clamp, compared with only a 4-fold suppression after 32 weeks of a HFD (Fig. 2E). Likewise, ketogenesis was incremented by 7-fold between the fasted and fed state in control mice, but it was barely responsive to nutritional state in 32-week HFD mice (Fig. 2F). These data indicate that ketogenesis occurs constitutively during hepatic insulin resistance but that severe insulin resistance (i.e., 32 weeks of HFD) blunts maximum ketogenesis. However, this modestly impaired fasting ketogenesis was still a 2-fold higher flux for acetyl-CoA than TCA cycle oxidation, indicating that β-oxidation remained in excess of respiratory requirements.

Progressing hepatic insulin resistance and steatosis dysregulates mitochondrial respiration

Because isotopomer analysis indicated increased hepatic oxidative flux, we determined whether fatty liver and

TABLE 3. Hepatic acylcarnitine levels in overnight-fasted mice on a high-fat diet

	8 Weeks			16 Weeks			32 Weeks		
	Control Diet	HFD	*P*	Control Diet	HFD	*P*	Control Diet	HFD	*P*
Free carnitine	1337 ± 91	1680 ± 260	0.17	1555 ± 65	1374 ± 144	0.13	1345 ± 223	1384 ± 151	0.44
C2	5.33 ± 1.4	6.74 ± 1.2	0.22	8.67 ± 1.2	13.2 ± 3.6	0.15	6.52 ± 1.7	26.5 ± 10	0.05
C3	3.75 ± 0.69	12.3 ± 5.1	0.07	8.93 ± 2.1	11.5 ± 4.05	0.29	2.16 ± 0.40	12.8 ± 2.9	0.006
C4	2.99 ± 1.0	2.79 ± 0.77	0.43	1.43 ± 0.18	4.23 ± 1.9	0.10	3.95 ± 0.66	12.0 ± 3.0	0.02
C5	0.25 ± 0.06	0.24 ± 0.04	0.43	0.28 ± 0.05	0.37 ± 0.06	0.29	1.37 ± 0.18	2.14 ± 0.23	0.01
C14	0.08 ± 0.02	0.04 ± 0.01	0.06	0.05 ± 0.01	0.05 ± 0.01	0.45	0.04 ± 0.004	0.06 ± 0.01	0.07
C16	0.49 ± 0.06	0.68 ± 0.2	0.20	0.34 ± 0.06	0.52 ± 0.12	0.18	0.52 ± 0.05	0.75 ± 0.1	0.04

Acylcarnitine (nmol/g protein) in liver. Data are represented as the mean ± SE (n = 6–8).

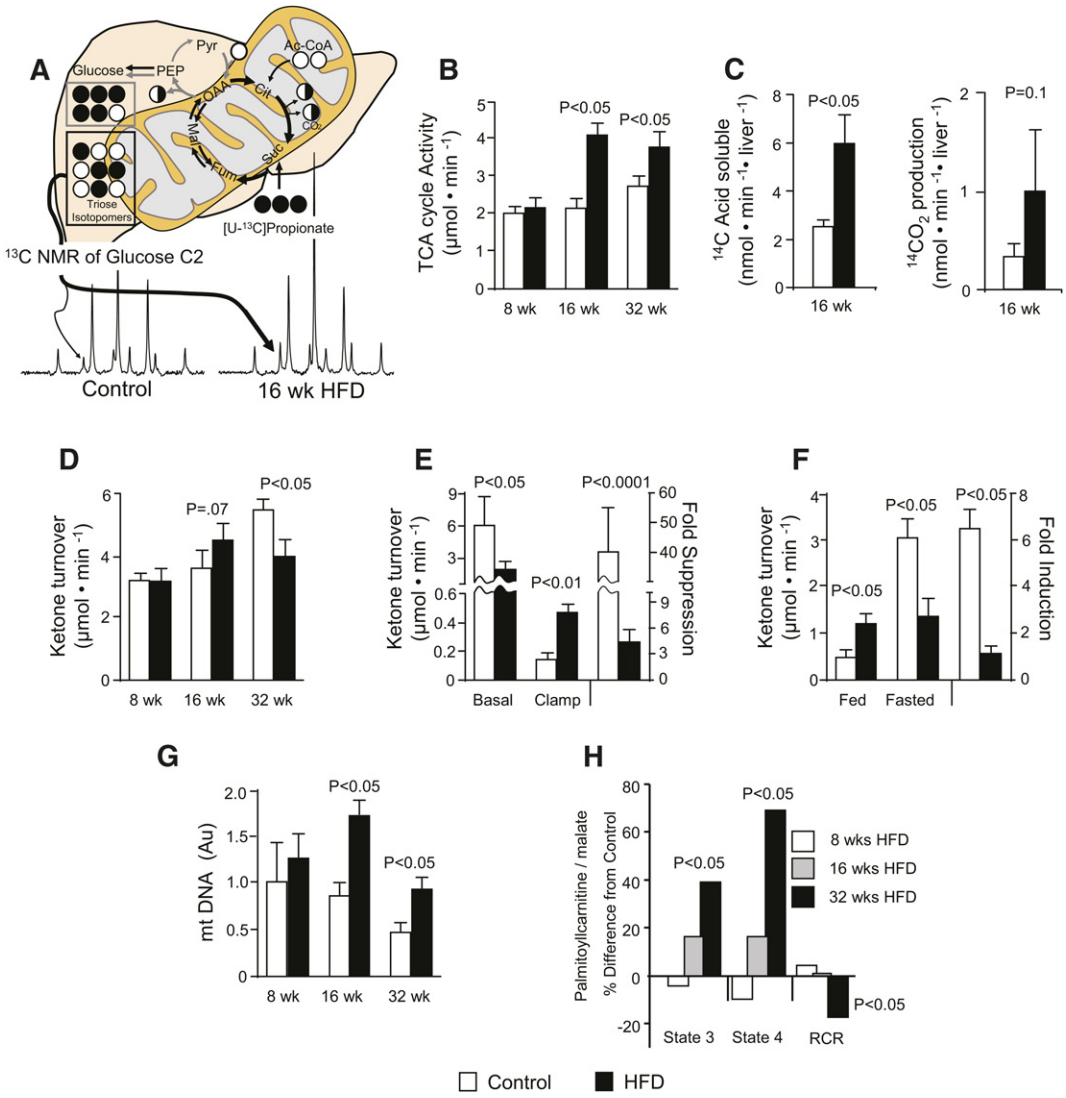

Fig. 2. Hepatic mitochondrial metabolism is elevated in HFD mice. (A) Carbon-13 isotopomer analysis of plasma glucose was used to evaluate hepatic fluxes relative to the TCA cycle after administration of [U-^{13}C]propionate as described by Landau et al. (46) and adapted to NMR analysis (48) for determination of absolute flux (41). See supplementary Table IV for isotopomer data. (B) In vivo hepatic mitochondrial TCA cycle flux in overnight-fasted mice (awake and unrestrained). (C) Oxidation of [1-^{14}C]palmitate in liver homogenates from 16-week-old HFD mice. (D) Determination of in vivo ketogenic flux by apparent turnover of [3,4-$^{13}C_2$]acetoacetate and [U-$^{13}C_4$]β-hydroxybutyrate. (E, F) Suppression of fasting in vivo ketogenesis by (E) euglycemic hyperinsulinemic clamp or (F) feeding. (G) Mitochondrial DNA content determined by real-time quantitative PCR. (H) Isolated mitochondrial respiration measured as O_2 consumption with palmitoylcarnitine/malate as substrate in the presence of no ADP (State 2), ADP (State 3), or ADP depletion (State 4) expressed as % difference from their respective age-matched control average (see supplementary Table VII for raw data). Data are presented as the mean ± SE (n = 4–8).

hepatic insulin resistance altered isolated mitochondrial function throughout 32 weeks of HFD. Quantification of mitochondrial DNA indicated elevated mitochondrial content in mice following 16 and 32 weeks on HFD relative to their age-matched controls (Fig. 2H). Isolated mitochondria oxidizing palmitoylcarnitine/malate during ADP-stimulated (state 3) and ADP-depleted (state 4) conditions tended to have increased O_2 consumption after 16 weeks of HFD and was markedly elevated after 32 weeks of HFD (Fig. 2G). These data are consistent with recent findings of upregulated hepatic mitochondrial respiration in HFD mice (24, 25) and humans with diabetes (27). Despite elevated respiration, the RCR was lower after 32 weeks of HFD with palmitoylcarnitine as a substrate, suggesting impaired coupling of oxidative metabolism and ATP synthesis (supplementary Table VII and Fig. 2G), and consistent with elevated expression of UCP2 (Table 2). Similar trends were obtained with succinate/rotenone and glutamate/malate (supplementary Table VII). Despite altered mitochondrial respiration, transmission electron microscopy did not identify morphologic defects, though mitochondria from HFD mice tended to be smaller (supplementary Fig. I-D). The data indicate that progressing insulin resistance is accompanied by elevated mitochondrial content

and increased in vitro respiration but that mitochondrial O_2 consumption and ATP synthesis are inefficiently coupled. These results are consistent with recent studies (18, 24, 25, 27) and suggest that elevated in vivo hepatic TCA cycle flux during insulin resistance may be required to compensate for reduced mitochondrial coupling efficiency.

Induction of oxidative metabolism marks the onset of oxidative stress and inflammation during hepatic insulin resistance

ROS production is a collateral consequence of mitochondrial respiration (60). Inasmuch as TCA cycle flux is a principal source of electrons for the respiratory chain, we examined whether the onset of oxidative stress and inflammation corresponded to the induction of TCA cycle function. Fasting liver ceramide content, a lipid metabolite that promotes both insulin resistance and inflammation (4), was elevated after 32 weeks of HFD (**Fig. 3A**). Superoxide dismutase activity in liver homogenates was higher in 32-week HFD mice (Fig. 3B), indicating heightened antioxidant response. Increased hepatic protein carbonylation after 16 weeks (Fig. 3C) and thiobarbituric acid reactive substance (TBARS) after 32 weeks (Fig. 3D) confirmed the onset ROS-mediated oxidative damage. It is not clear why protein carbonylation was evident before other markers of oxidative stress, but it might be due to transient factors, such as fasting status. Nonetheless, hepatocellular damage at 16 weeks was consistent with elevated hepatic mRNA levels of *IL6*, *Tnfα*, and *Cox-2/Ptgs2* (Fig. 3E–G), which might be an inflammatory response to oxidative damage. Histologic evidence of liver inflammation did not appear until 32 weeks of HFD, as indicated by lymphocytic infiltration in HE-stained sections of liver (Fig. 3H). In contrast, circulating interlukins (supplementary Fig. I-E) were increased by 8 weeks, in agreement with the rapid affect of obesity on adipose inflammation (14, 16). Overall, the induction of oxidative stress and inflammation during hepatic insulin resistance is consistent with previous data (5, 8–12, 17, 18). The common timing is consistent with ROS production originating with elevated TCA cycle flux and a concomitant electron load to a dysfunctional respiratory chain.

DISCUSSION

The putative role of dysregulated intracellular lipid catabolism in the mechanism of insulin resistance and NAFLD led us to investigate mitochondrial TCA cycle metabolism in the liver of mice developing hepatic insulin resistance and fatty liver. The findings of this study indicate that lipid accumulation and loss of insulin action result in elevated oxidative and anaplerotic pathways of the hepatic TCA cycle. The initial rise in mitochondrial TCA cycle metabolism coincided precisely with the loss of Foxo1 phosphorylation. Thus, one potential metabolic mechanism by which TCA cycle function is elevated during insulin resistance follows from the dysregulation of insulin-regulated biosynthetic pathways that require TCA cycle function for substrate or energetic potential. Gluconeogenesis from TCA cycle precursors was elevated, and there was a marked increase in flux through the anaplerotic/cataplerotic pathways of the TCA cycle. Although impaired insulin action during a HFD did not result in elevated PEPCK expression, this appears to be a common feature of HFD rodents (57). However, G6Pase expression was increased, and although PC expression was normal, elevated acetylcarnitine was consistent with the known posttranslational activation of PC by acetyl-CoA and fat oxidation (58). This is also teleologically consistent with the known metabolic activation of gluconeogenesis by oxidative metabolism via *(i)* formation of citrate by the TCA cycle, which allosterically inhibits glycolysis; *(ii)* generation of cofactors (NADH and ATP) required for the reactions of gluconeogenesis; and *(iii)* allosteric activation of PC by acetyl-CoA (58, 61). In agreement with these metabolic factors, the anaplerotic and oxidative fluxes of the TCA cycle are reciprocally regulated in the liver of humans and mice (47, 62), suggesting that the induction of gluconeogenesis by impaired insulin action may stimulate oxidative metabolism.

Elevated TCA cycle flux is also likely incited by dysfunctional mitochondrial respiration, especially during later stages of hepatic insulin resistance. Loss of insulin action is reported to degrade respiratory complexes 1 and 3 via downstream targets of Foxo1 (22), which might account for impaired mitochondrial function during a HFD. The alterations in isolated mitochondrial function observed here are generally consistent with previous reports of increased expression of respiratory proteins, oxidative capacity, uncoupled respiration, and impaired membrane potential in similar mouse models of insulin resistance (18, 24, 25), and with impaired hepatic ATP synthesis (3, 20) in humans with insulin resistance. Mitochondrial dysfunction is somewhat paradoxical in the setting of increased gluconeogenesis, as this pathway traverses the mitochondria and requires mitochondrial-derived NADH and ATP for a number of its steps. However, elevated TCA cycle flux partially resolves the paradox by supplying increased $NADH/FADH_2$ as compensation for dysfunctional respiration and by providing increased cataplerotic substrates to support overactive synthetic pathways. Although we found elevated TCA cycle function (16 weeks) to predate respiratory dysfunction in isolated mitochondria (32 weeks), it is possible that the latter was present even earlier, as reported in other studies (18, 24, 25) but not detected in our particular experimental protocol (i.e., fasting state, mitochondrial isolation procedure, etc.).

The molecular mechanism responsible for increased TCA cycle metabolism was not completely evident from analysis of gene expression. PGC-1α was mildly induced at 16 weeks, which is consistent with loss of Akt and Foxo1 phosphorylation and with our previous finding that PGC-1α is required for optimal TCA cycle function (63). However, it was not elevated after 32 weeks of HFD, and other regulators or metabolic enzymes of fat oxidation were actually decreased, which is qualitatively similar to other findings in HFD mice (64). Downregulated fat oxidation during severe insulin resistance has been linked to impaired

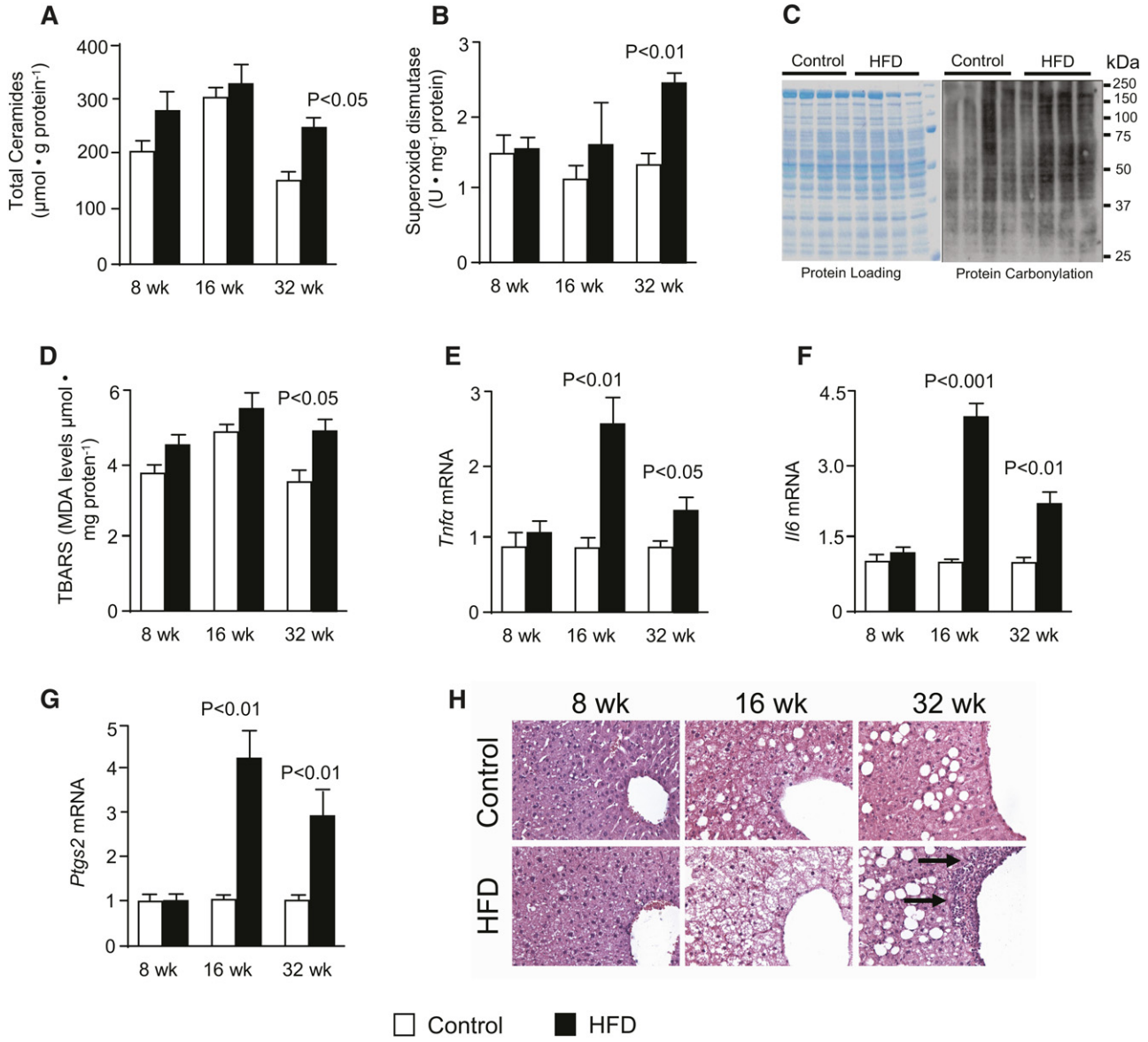

Fig. 3. Markers of oxidative stress and inflammation are elevated with the same timing as increased oxidative metabolism in the liver of HFD mice. (A) Total ceramide levels in the liver measured by LC-MS/MS analysis; (B) superoxide dismutase activity measured in liver homogenates; (C) carbonylation of proteins in lysates from crude liver mitochondria with Coomasie-stained gel as loading control; (D) lipid peroxidation assessed by analysis of TBARS; (E–H) relative gene expression analysis of (E) *Il6,* (F) *Tnfa*, and (G) *Ptgs2*, and (H) Hematoxylin-stained liver sections with arrows indicating macrophage infiltration (original magnification ×20; n = 2) in overnight-fasted mice fed either a control or high-fat diet for 8, 16, and 32 weeks. Data are presented as the mean ± SE (n = 6–8) unless otherwise noted.

SIRT1 activity and deactivated PGC-1α (but not reduced expression) (23). Impaired SIRT3 activity during hepatic insulin resistance may also reduce the activity of enzymes of lipid oxidation (29). In agreement with those data, we found that fasting ketogenesis was mildly suppressed at 32 weeks of HFD and markedly suppressed in more severely insulin-resistant models (39). Thus maximal β-oxidation may be blunted during severe insulin resistance (32 weeks) compared with a moderate condition (16 weeks) where it is actually increased. Despite blunted fasting ketogenesis, its suppression by feeding and clamp was diminished, suggesting constitutively active β-oxidation in the prandial state and loss of the normal metabolic flexibility of hepatic fat oxidation.

Elevated fasting TCA cycle flux during severe insulin resistance appears to contradict impaired fasting ketogenesis and the suppression of some β-oxidation genes. We suspect that the canonical autoregulation of TCA cycle function by cellular energy status (30) is a dominant factor that induces TCA cycle flux under conditions of respiratory uncoupling and increased biosynthetic demand, even in the setting of impaired ketogenesis. In this regard, it is important to note that fasting β-oxidation greatly exceeds hepatocellular energy requirements, with excess acetyl-CoA shunted to ketogenesis rather than being oxidized in the TCA cycle (31). In other words, the TCA cycle oxidizes the acetyl-CoA required for cellular energy homeostasis, so fasting ketogenesis is much more pliable to the effects

of dysregulated β-oxidation. To put this in perspective, despite a 30% reduction in ketogenesis and a 40% increase in TCA cycle oxidation, 32-week HFD mice still dispose two-thirds of their acetyl-CoA via ketogenesis, and acetylcarnitine is actually elevated. We deduce from these data that impaired β-oxidation can occur with severe insulin resistance, but under most circumstances, oxidative flux in the hepatic TCA cycle is not at risk of being limited.

Elevated TCA cycle flux during insulin resistance indicates a marked increase in electron deposition into the respiratory chain, which might be an important element in the known link between oxidative stress, inflammation, and hepatic insulin resistance (5, 9). The simultaneous appearance of impaired AKT phosphorylation, inflammatory cytokine expression, and increased oxidative flux may indicate a common metabolic etiology. Coordinately increased TCA cycle flux and impaired mitochondrial respiratory efficiency is consistent with elevated oxygen demand, which has been suggested to potentiate hypoxia-related ROS production and cell damage in a similar model (18). The production of ROS associated with elevated fat oxidation causes insulin resistance by activation of NF-κB- and/or JNK-mediated IRS phosphorylation (12, 16), a process which can be ameliorated by suppressing β-oxidation in cell systems (13). An isotopomer study carried out in liver cells treated with palmitate also specifically demonstrated that elevated TCA cycle function was sufficient to mediate cell damage and lipoapoptosis (65). Such cellular stresses are known to recruit proinflammatory macrophages (14), and this process appears to be required for diet-induced hepatic insulin resistance (15). Whether or not elevated oxidative metabolism predates the development of inflammation remains unanswered. We suspect that even at 8 weeks, unrepressed oxidative flux in the fed state might hasten the inflammatory process and potentiate insulin resistance.

As in mice, whether or not hepatic insulin resistance results in dysregulated oxidative flux in humans probably depends on the degree of insulin resistance and the nutritional status of the individual. Based on the data of this study, it is not surprising that both elevated (8) and reduced ketones (66) have been identified in individuals with various manifestations of hepatic insulin resistance. However, because the TCA cycle is somewhat autonomous of ketogenesis, it is difficult to extrapolate these findings to the function of oxidative metabolism during insulin resistance or NAFLD. The degree of respiratory defects and elevated biosynthetic pathways, such as gluconeogenesis or proliferation, may also be important determinants of TCA cycle function in people with insulin resistance and/or NAFLD. Positron emission tomography studies indicated that obese humans have increased total β-oxidation (ketogenesis and TCA cycle oxidation) (67). We recently investigated individuals with hepatic insulin resistance and NAFLD and found that ketogenesis was normal but that the TCA cycle had increased anaplerotic and oxidative fluxes that correlated with the degree of liver fat (68). These data indicate that limitations in fat oxidation are unlikely to contribute to hepatic lipid accumulation, but in combination with the mouse data, suggest that the collateral oxidative stress caused by this process may be important in progression of NAFLD. This is a well-covered topic within the field of NAFLD, with most attention issued to the role of respiratory chain defects in ROS production. The present data highlight regulatory defects of TCA cycle function as a source of increased electron deposition to a ROS-prone respiratory chain.

In conclusion, the metabolic events during the progression of diet-induced hepatic insulin proceed from *i*) metabolic overload of lipid and initiation of hepatic insulin resistance; *ii*) loss of insulin-mediated suppression of gluconeogenesis and mitochondrial TCA cycle metabolism; and *iii*) impaired mitochondrial efficiency, oxidative stress, inflammation, and hepatocellular damage associated with chronic insulin resistance and fatty liver disease. The causal factors linking these processes remain to be identified, but induction of the mitochondrial TCA cycle appears to metabolically enable, if not instigate, mitochondrial dysfunction and oxidative stress during hepatic insulin resistance.

The authors are grateful to Dr. Christopher J. Gilpin and the Molecular and Cellular Imaging Facility at the University of Texas Southwestern Medical Center for assistance with mitochondrial morphology. João A.G. Duarte provided valuable assistance with biochemical assays.

REFERENCES

1. Muoio, D. M., and C. B. Newgard. 2008. Mechanisms of disease: molecular and metabolic mechanisms of insulin resistance and beta-cell failure in type 2 diabetes. *Nat. Rev. Mol. Cell Biol.* **9:** 193–205.
2. Savage, D. B., K. F. Petersen, and G. I. Shulman. 2007. Disordered lipid metabolism and the pathogenesis of insulin resistance. *Physiol. Rev.* **87:** 507–520.
3. Szendroedi, J., E. Phielix, and M. Roden. 2011. The role of mitochondria in insulin resistance and type 2 diabetes mellitus. *Nat. Rev. Endocrinol.* **8:** 92–103.
4. Summers, S. A. 2006. Ceramides in insulin resistance and lipotoxicity. *Prog. Lipid Res.* **45:** 42–72.
5. Cusi, K. 2009. Role of insulin resistance and lipotoxicity in non-alcoholic steatohepatitis. *Clin. Liver Dis.* **13:** 545–563.
6. Zhang, D., Z. X. Liu, C. S. Choi, L. Tian, R. Kibbey, J. Dong, G. W. Cline, P. A. Wood, and G. I. Shulman. 2007. Mitochondrial dysfunction due to long-chain acyl-CoA dehydrogenase deficiency causes hepatic steatosis and hepatic insulin resistance. *Proc. Natl. Acad. Sci. USA.* **104:** 17075–17080.
7. Samuel, V. T., Z-X. Liu, X. Qu, B. D. Elder, S. Bilz, D. Befroy, A. J. Romanelli, and G. I. Shulman. 2004. Mechanism of hepatic insulin resistance in non-alcoholic fatty liver disease. *J. Biol. Chem.* **279:** 32345–32353.
8. Sanyal, A. J., C. Campbell-Sargent, F. Mirshahi, W. B. Rizzo, M. J. Contos, R. K. Sterling, V. A. Luketic, M. L. Shiffman, and J. N. Clore. 2001. Nonalcoholic steatohepatitis: association of insulin resistance and mitochondrial abnormalities. *Gastroenterology.* **120:** 1183–1192.
9. Serviddio, G., F. Bellanti, R. Tamborra, T. Rollo, N. Capitanio, A. D. Romano, J. Sastre, G. Vendemiale, and E. Altomare. 2008. Uncoupling protein-2 (UCP2) induces mitochondrial proton leak and increases susceptibility of non-alcoholic steatohepatitis (NASH) liver to ischaemia-reperfusion injury. *Gut.* **57:** 957–965.
10. Pessayre, D., and B. Fromenty. 2005. NASH: a mitochondrial disease. *J. Hepatol.* **42:** 928–940.
11. Day, C. P., and O. F. James. 1998. Steatohepatitis: a tale of two "hits"? *Gastroenterology.* **114:** 842–845.

12. Gao, D., S. Nong, X. Huang, Y. Lu, H. Zhao, Y. Lin, Y. Man, S. Wang, J. Yang, and J. Li. 2010. The effects of palmitate on hepatic insulin resistance are mediated by NADPH Oxidase 3-derived reactive oxygen species through JNK and p38MAPK pathways. *J. Biol. Chem.* **285:** 29965–29973.
13. Nakamura, S., T. Takamura, N. Matsuzawa-Nagata, H. Takayama, H. Misu, H. Noda, S. Nabemoto, S. Kurita, T. Ota, H. Ando, et al. 2009. Palmitate induces insulin resistance in H4IIEC3 hepatocytes through reactive oxygen species produced by mitochondria. *J. Biol. Chem.* **284:** 14809–14818.
14. Chawla, A., K. D. Nguyen, and Y. P. S. Goh. 2011. Macrophage-mediated inflammation in metabolic disease. *Nat. Rev. Immunol.* **11:** 738–749.
15. Huang, W., A. Metlakunta, N. Dedousis, P. Zhang, I. Sipula, J. J. Dube, D. K. Scott, and R. M. O'Doherty. 2010. Depletion of liver Kupffer cells prevents the development of diet-induced hepatic steatosis and insulin resistance. *Diabetes.* **59:** 347–357.
16. Hotamisligil, G. S. 2006. Inflammation and metabolic disorders. *Nature.* **444:** 860–867.
17. Caldwell, S. H., L. A. R. de Freitas, S. H. Park, M. L. V. Moreno, J. A. Redick, C. A. Davis, B. J. Sisson, J. T. Patrie, H. Cotrim, C. K. Argo, et al. 2009. Intramitochondrial crystalline inclusions in nonalcoholic steatohepatitis. *Hepatology.* **49:** 1888–1895.
18. Mantena, S. K., D. P. Vaughn, K. K. Andringa, H. B. Eccleston, A. L. King, G. A. Abrams, J. E. Doeller, D. W. Kraus, V. M. Darley-Usmar, and S. M. Bailey. 2009. High fat diet induces dysregulation of hepatic oxygen gradients and mitochondrial function in vivo. *Biochem. J.* **417:** 183–193.
19. Cortez-Pinto, H., J. Chatham, V. P. Chacko, C. Arnold, A. Rashid, and A. M. Diehl. 1999. Alterations in liver ATP homeostasis in human nonalcoholic steatohepatitis. *JAMA.* **282:** 1659–1664.
20. Szendroedi, J., M. Chmelik, A. I. Schmid, P. Nowotny, A. Brehm, M. Krssak, E. Moser, and M. Roden. 2009. Abnormal hepatic energy homeostasis in type 2 diabetes. *Hepatology.* **50:** 1079–1086.
21. Gross, D. N., A. P. J. van den Heuvel, and M. J. Birnbaum. 2008. The role of FoxO in the regulation of metabolism. *Oncogene.* **27:** 2320–2336.
22. Cheng, Z., S. Guo, K. Copps, X. Dong, R. Kollipara, J. T. Rodgers, R. A. Depinho, P. Puigserver, and M. F. White. 2009. Foxo1 integrates insulin signaling with mitochondrial function in the liver. *Nat. Med.* **15:** 1307–1311.
23. Cheng, Z., and M. F. White. 2011. Targeting Forkhead box O1 from the concept to metabolic diseases: lessons from mouse models. *Antioxid. Redox Signal.* **14:** 649–661.
24. Poussin, C., M. Ibberson, D. Hall, J. Ding, J. Soto, E. D. Abel, and B. Thorens. 2011. Oxidative phosphorylation flexibility in the liver of mice resistant to high-fat diet–induced hepatic steatosis. *Diabetes.* **60:** 2216–2224.
25. Buchner, D. A., S. N. Yazbek, P. Solinas, L. C. Burrage, M. G. Morgan, C. L. Hoppel, and J. H. Nadeau. 2011. Increased mitochondrial oxidative phosphorylation in the liver is associated with obesity and insulin resistance. *Obesity (Silver Spring).* **19:** 917–924.
26. Sunny, N. E., S. Satapati, X. Fu, T. He, R. Mehdibeigi, C. Spring-Robinson, J. Duarte, M. J. Potthoff, J. D. Browning, and S. C. Burgess. 2010. Progressive adaptation of hepatic ketogenesis in mice fed a high-fat diet. *Am. J. Physiol. Endocrinol. Metab.* **298:** E1226–E1235.
27. Takamura, T., H. Misu, N. Matsuzawa-Nagata, M. Sakurai, T. Ota, A. Shimizu, S. Kurita, Y. Takeshita, H. Ando, M. Honda, et al. 2008. Obesity upregulates genes involved in oxidative phosphorylation in livers of diabetic patients. *Obesity (Silver Spring).* **16:** 2601–2609.
28. Choudhury, M., K. R. Jonscher, and J. E. Friedman. 2011. Reduced mitochondrial function in obesity-associated fatty liver: SIRT3 takes on the fat. *Aging (Albany NY).* **3:** 175–178.
29. Kendrick, A. A., M. Choudhury, S. M. Rahman, C. E. McCurdy, M. Friederich, J. L. K. Van Hove, P. A. Watson, N. Birdsey, J. J. Bao, D. Gius, et al. 2011. Fatty liver is associated with reduced SIRT3 activity and mitochondrial protein hyperacetylation. *Biochem. J.* **433:** 505–514.
30. Krebs, H. A. 1970. Rate control of the tricarboxylic acid cycle. *Adv. Enzyme Regul.* **8:** 335–353.
31. McGarry, J. D., and D. W. Foster. 1980. Regulation of hepatic fatty acid oxidation and ketone body production. *Annu. Rev. Biochem.* **49:** 395–420.
32. Owen, O. E., S. C. Kalhan, and R. W. Hanson. 2002. The key role of anaplerosis and cataplerosis for citric acid cycle function. *J. Biol. Chem.* **277:** 30409–30412.
33. Magnusson, I., D. L. Rothman, L. D. Katz, R. G. Shulman, and G. I. Shulman. 1992. Increased rate of gluconeogenesis in type II diabetes mellitus. A 13C nuclear magnetic resonance study. *J. Clin. Invest.* **90:** 1323–1327.
34. Chevalier, S., S. C. Burgess, C. R. Malloy, R. Gougeon, E. B. Marliss, and J. A. Morais. 2006. The greater contribution of gluconeogenesis to glucose production in obesity is related to increased whole-body protein catabolism. *Diabetes.* **55:** 675–681.
35. Diraison, F., P. Moulin, and M. Beylot. 2003. Contribution of hepatic de novo lipogenesis and reesterification of plasma non esterified fatty acids to plasma triglyceride synthesis during non-alcoholic fatty liver disease. *Diabetes Metab.* **29:** 478–485.
36. Magnusson, I., W. C. Schumann, G. E. Bartsch, V. Chandramouli, K. Kumaran, J. Wahren, and B. R. Landau. 1991. Noninvasive tracing of Krebs cycle metabolism in liver. *J. Biol. Chem.* **266:** 6975–6984.
37. Des Rosiers, C., J. A. Montgomery, M. Garneau, F. David, O. A. Mamer, P. Daloze, G. Toffolo, C. Cobelli, B. R. Landau, and H. Brunengraber. 1990. Pseudoketogenesis in hepatectomized dogs. *Am. J. Physiol.* **258:** E519–E528.
38. Bailey, J. W., M. W. Haymond, and J. M. Miles. 1990. Validation of two-pool model for in vivo ketone body kinetics. *Am. J. Physiol.* **258:** E850–E855.
39. Satapati, S., T. He, T. Inagaki, M. Potthoff, M. E. Merritt, V. Esser, D. J. Mangelsdorf, S. A. Kliewer, J. D. Browning, and S. C. Burgess. 2008. Partial resistance to peroxisome proliferator-activated receptor-alpha agonists in ZDF rats is associated with defective hepatic mitochondrial metabolism. *Diabetes.* **57:** 2012–2021.
40. Burgess, S. C., F. M. H. Jeffrey, C. Storey, A. Milde, N. Hausler, M. E. Merritt, H. Mulder, C. Holm, A. D. Sherry, and C. R. Malloy. 2005. Effect of murine strain on metabolic pathways of glucose production after brief or prolonged fasting. *Am. J. Physiol. Endocrinol. Metab.* **289:** E53–E61.
41. Jin, E. S., J. G. Jones, M. E. Merritt, S. C. Burgess, C. R. Malloy, and A. D. Sherry. 2004. Glucose production, gluconeogenesis, and hepatic tricarboxylic acid cycle fluxes measured by nuclear magnetic resonance analysis of a single glucose derivative. *Anal. Biochem.* **327:** 149–155.
42. Jin, E. S., J. G. Jones, S. C. Burgess, M. E. Merritt, A. D. Sherry, and C. R. Malloy. 2005. Comparison of [3,4–13C2]glucose to [6,6–2H2] glucose as a tracer for glucose turnover by nuclear magnetic resonance. *Magn. Reson. Med.* **53:** 1479–1483.
43. Landau, B. R., J. Wahren, V. Chandramouli, W. C. Schumann, K. Ekberg, and S. C. Kalhan. 1996. Contributions of gluconeogenesis to glucose production in the fasted state. *J. Clin. Invest.* **98:** 378–385.
44. Burgess, S. C., M. Nuss, V. Chandramouli, D. S. Hardin, M. Rice, B. R. Landau, C. R. Malloy, and A. D. Sherry. 2003. Analysis of gluconeogenic pathways in vivo by distribution of 2H in plasma glucose: comparison of nuclear magnetic resonance and mass spectrometry. *Anal. Biochem.* **318:** 321–324.
45. Rémésy, C., C. Demigne, and F. Chartier. 1980. Origin and utilization of volatile fatty acids in the rat. *Reprod. Nutr. Dev.* **20:** 1339–1349.
46. Landau, B. R., W. C. Schumann, V. Chandramouli, I. Magnusson, K. Kumaran, and J. Wahren. 1993. 14C-labeled propionate metabolism in vivo and estimates of hepatic gluconeogenesis relative to Krebs cycle flux. *Am. J. Physiol.* **265:** E636–E647.
47. Browning, J. D., B. Weis, J. Davis, S. Satapati, M. Merritt, C. R. Malloy, and S. C. Burgess. 2008. Alterations in hepatic glucose and energy metabolism as a result of calorie and carbohydrate restriction. *Hepatology.* **48:** 1487–1496.
48. Jones, J. G., R. Naidoo, A. D. Sherry, F. M. H. Jeffrey, G. L. Cottam, and C. R. Malloy. 1997. Measurement of gluconeogensis and pyruvate recycling in the rat liver: a simple analysis of glucose and glutamate isotopomers during metabolism of [1,2,3-^{13}C3]propionate. *FEBS Lett.* **412:** 131–137.
49. Sherry, A. D., F. M. H. Jeffrey, and C. R. Malloy. 2004. Analytical solutions of 13C isotopomer analysis of complex metabolic conditions: substrate oxidation, multiple pyruvate cycles, and gluconeogenesis. *Metab. Eng.* **6:** 12–24.
50. Dohm, G. L., R. L. Huston, E. W. Askew, and P. C. Weiser. 1972. Effects of exercise on activity of heart and muscle mitochondria. *Am. J. Physiol.* **223:** 783–787.
51. Matsuda, M., and R. A. DeFronzo. 1999. Insulin sensitivity indices obtained from oral glucose tolerance testing: comparison with the euglycemic insulin clamp. *Diabetes Care.* **22:** 1462–1470.

52. Potthoff, M. J., J. Boney-Montoya, M. Choi, T. He, N. E. Sunny, S. Satapati, K. Suino-Powell, H. E. Xu, R. D. Gerard, B. N. Finck, et al. 2011. FGF15/19 regulates hepatic glucose metabolism by inhibiting the CREB-PGC-1[alpha] pathway. *Cell Metab.* **13:** 729–738.
53. An, J., D. M. Muoio, M. Shiota, Y. Fujimoto, G. W. Cline, G. I. Shulman, T. R. Koves, R. Stevens, D. Millington, and C. B. Newgard. 2004. Hepatic expression of malonyl-CoA decarboxylase reverses muscle, liver and whole-animal insulin resistance. *Nat. Med.* **10:** 268–274.
54. Lieser, B., G. Liebisch, W. Drobnik, and G. Schmitz. 2003. Quantification of sphingosine and sphinganine from crude lipid extracts by HPLC electrospray ionization tandem mass spectrometry. *J. Lipid Res.* **44:** 2209–2216.
55. Frezza, C., S. Cipolat, and L. Scorrano. 2007. Organelle isolation: functional mitochondria from mouse liver, muscle and cultured filroblasts. *Nat. Protoc.* **2:** 287–295.
56. Groen, A. K., C. W. van Roermund, R. C. Vervoorn, and J. M. Tager. 1986. Control of gluconeogenesis in rat liver cells. Flux control coefficients of the enzymes in the gluconeogenic pathway in the absence and presence of glucagon. *Biochem. J.* **237:** 379–389.
57. Samuel, V. T., S. A. Beddow, T. Iwasaki, X-M. Zhang, X. Chu, C. D. Still, G. S. Gerhard, and G. I. Shulman. 2009. Fasting hyperglycemia is not associated with increased expression of PEPCK or G6Pc in patients with Type 2 Diabetes. *Proc. Natl. Acad. Sci. USA.* **106:** 12121–12126.
58. Williamson, J. R., R. A. Kreisberg, and P. W. Felts. 1966. Mechanism for the stimulation of gluconeogenesis by fatty acids in perfused rat liver. *Proc. Natl. Acad. Sci. USA.* **56:** 247–254.
59. Koves, T. R., J. R. Ussher, R. C. Noland, D. Slentz, M. Mosedale, O. Ilkayeva, J. Bain, R. Stevens, J. R. Dyck, C. B. Newgard, et al. 2008. Mitochondrial overload and incomplete fatty acid oxidation contribute to skeletal muscle insulin resistance. *Cell Metab.* **7:** 45–56.
60. Murphy, M. P. 2009. How mitochondria produce reactive oxygen species. *Biochem. J.* **417:** 1–13.
61. Williamson, J. R., and R. H. Cooper. 1980. Regulation of the citric acid cycle in mammalian systems. *FEBS Lett.* **117(Suppl.):** K73–K85.
62. Burgess, S. C., T. He, Z. Yan, J. Lindner, A. D. Sherry, C. R. Malloy, J. D. Browning, and M. A. Magnuson. 2007. Cytosolic phosphoenolpyruvate carboxykinase does not solely control the rate of hepatic gluconeogenesis in the intact mouse liver. *Cell Metab.* **5:** 313–320.
63. Burgess, S. C., T. C. Leone, A. R. Wende, M. A. Croce, Z. Chen, A. D. Sherry, C. R. Malloy, and B. N. Finck. 2006. Diminished hepatic gluconeogenesis via defects in tricarboxylic acid cycle flux in peroxisome proliferator-activated receptor gamma coactivator-1alpha (PGC-1alpha)-deficient mice. *J. Biol. Chem.* **281:** 19000–19008.
64. Chan, M-Y., Y. Zhao, and C-K. Heng. 2008. Sequential responses to high-fat and high-calorie feeding in an obese mouse model. *Obesity (Silver Spring).* **16:** 972–978.
65. Noguchi, Y., J. D. Young, J. O. Aleman, M. E. Hansen, J. K. Kelleher, and G. Stephanopoulos. 2009. Effect of anaplerotic fluxes and amino acid availability on hepatic lipoapoptosis. *J. Biol. Chem.* **284:** 33425–33436.
66. Bickerton, A. S., R. Roberts, B. A. Fielding, H. Tornqvist, E. E. Blaak, A. J. Wagenmakers, M. Gilbert, S. M. Humphreys, F. Karpe, and K. N. Frayn. 2008. Adipose tissue fatty acid metabolism in insulin-resistant men. *Diabetologia.* **51:** 1466–1474.
67. Iozzo, P., M. Bucci, A. Roivainen, K. Någren, M. J. Järvisalo, J. Kiss, L. Guiducci, B. Fielding, A. G. Naum, R. Borra, et al. 2010. Fatty acid metabolism in the liver, measured by positron emission tomography, is increased in obese individuals. *Gastroenterology.* **139:** 846–856.
68. Sunny, N. E., E. J. Parks, J. D. Browning, and S. C. Burgess. 2011. Excessive hepatic mitochondrial TCA cycle and gluconeogenesis in humans with nonalcoholic fatty liver disease. *Cell Metab.* **14:** 804–810.